Research Article | Vol. 8, No. 6 | 1 Jun 2017 | BIOMEDICAL OPTICS EXPRESS 3045
Biomedical Optics EXPRESS

Noninvasive mesoscopic imaging of actinic skin damage using spatial frequency domain imaging

JEFFREY B. TRAVERS,[1,2,3,5] CHIEN POON,[4,5] DANIEL J. ROHRBACH,[4] NATHAN M. WEIR,[2] ELIZABETH CATES,[1] FAYE HAGER,[1] AND ULAS SUNAR[4,*]

[1]*Department of Pharmacology & Toxicology, Boonshoft School of Medicine, Wright State University, Dayton, OH 45435, USA*
[2]*Department of Dermatology, Boonshoft School of Medicine, Wright State University, Dayton, OH 45435, USA*
[3]*Dayton Veterans Administration Medical Center, Dayton, OH 45428, USA*
[4]*Department of Biomedical, Industrial & Human Factors Engineering, Wright State University, Dayton, OH 45435, USA*
[5] *These authors contributed equally to this manuscript.*
[*]*ulas.sunar@wright.edu*

Abstract: For prevention and accurate intervention planning, it is crucial to predict if lesions will progress towards cancer. In this study, we investigated the change in optical properties and vascular parameters to characterize skin tissue from mild photodamage to actinic keratosis (AK). Multi-wavelength spatial frequency domain imaging (SFDI) measurements were performed on three patients with clinically normal skin, as well as pre-cancerous actinic keratosis lesions. Our results indicate that there exist significant differences in both optical and vascular parameters between these patients, and that these parameters can be early biomarkers of neoplasia. Ultimately, clinicians can use this noninvasive approach for frequent monitoring of high-risk population.

OCIS codes: (170.0110) Imaging systems; (170.1870) Dermatology; (170.6935) Tissue characterization; (110.4234) Multispectral and hyperspectral imaging

References and links

1. H. W. Rogers, M. A. Weinstock, S. R. Feldman, and B. M. Coldiron, "Incidence Estimate of Nonmelanoma Skin Cancer (Keratinocyte Carcinomas) in the U.S. Population, 2012," JAMA Dermatol. **151**(10), 1081–1086 (2015).
2. C. Kim, J. Cheng, and O. R. Colegio, "Cutaneous squamous cell carcinomas in solid organ transplant recipients: emerging strategies for surveillance, staging, and treatment," Semin. Oncol. **43**(3), 390–394 (2016).
3. R. N. Werner, E. Stockfleth, S. M. Connolly, O. Correia, R. Erdmann, P. Foley, A. K. Gupta, A. Jacobs, H. Kerl, H. W. Lim, G. Martin, M. Paquet, D. M. Pariser, S. Rosumeck, H. J. Röwert-Huber, A. Sahota, O. P. Sangueza, S. Shumack, B. Sporbeck, N. A. Swanson, L. Torezan, and A. Nast; International League of Dermatological Societies; European Dermatology Forum, "Evidence- and consensus-based (S3) Guidelines for the Treatment of Actinic Keratosis - International League of Dermatological Societies in cooperation with the European Dermatology Forum - Short version," J. Eur. Acad. Dermatol. Venereol. **29**(11), 2069–2079 (2015).
4. S. T. Guenthner, R. M. Hurwitz, L. J. Buckel, and H. R. Gray, "Cutaneous squamous cell carcinomas consistently show histologic evidence of in situ changes: a clinicopathologic correlation," J. Am. Acad. Dermatol. **41**(3), 443–448 (1999).
5. M. Rajadhyaksha, A. Marghoob, A. Rossi, A. C. Halpern, and K. S. Nehal, "Reflectance confocal microscopy of skin in vivo: From bench to bedside," Lasers Surg. Med. **49**(1), 7–19 (2017).
6. A. Marneffe, M. Suppa, M. Miyamoto, V. Del Marmol, and M. Boone, "Validation of a diagnostic algorithm for the discrimination of actinic keratosis from normal skin and squamous cell carcinoma by means of high-definition optical coherence tomography," Exp. Dermatol. **25**(9), 684–687 (2016).
7. J. Olsen, L. Themstrup, N. De Carvalho, M. Mogensen, G. Pellacani, and G. B. Jemec, "Diagnostic accuracy of optical coherence tomography in actinic keratosis and basal cell carcinoma," Photodiagn. Photodyn. Ther. **16**, 44–49 (2016).
8. R. B. Saager, D. J. Cuccia, S. Saggese, K. M. Kelly, and A. J. Durkin, "A light emitting diode (LED) based spatial frequency domain imaging system for optimization of photodynamic therapy of nonmelanoma skin cancer: quantitative reflectance imaging," Lasers Surg. Med. **45**(4), 207–215 (2013).

#291668 https://doi.org/10.1364/BOE.8.003045
Journal © 2017 Received 29 Mar 2017; revised 8 May 2017; accepted 9 May 2017; published 23 May 2017

Biomedical Optics EXPRESS

9. T. J. Muldoon, S. A. Burgess, B. R. Chen, D. Ratner, and E. M. Hillman, "Analysis of skin lesions using laminar optical tomography," Biomed. Opt. Express **3**(7), 1701–1712 (2012).
10. M. S. Ozturk, C. W. Chen, R. Ji, L. Zhao, B. N. Nguyen, J. P. Fisher, Y. Chen, and X. Intes, "Mesoscopic Fluorescence Molecular Tomography for Evaluating Engineered Tissues," Ann. Biomed. Eng. **44**(3), 667–679 (2016).
11. M. S. Ozturk, D. Rohrbach, U. Sunar, and X. Intes, "Mesoscopic fluorescence tomography of a photosensitizer (HPPH) 3D biodistribution in skin cancer," Acad. Radiol. **21**(2), 271–280 (2014).
12. D. J. Cuccia, F. Bevilacqua, A. J. Durkin, F. R. Ayers, and B. J. Tromberg, "Quantitation and mapping of tissue optical properties using modulated imaging," J. Biomed. Opt. **14**(2), 024012 (2009).
13. D. J. Cuccia, F. Bevilacqua, A. J. Durkin, and B. J. Tromberg, "Modulated imaging: quantitative analysis and tomography of turbid media in the spatial-frequency domain," Opt. Lett. **30**(11), 1354–1356 (2005).
14. R. B. Saager, D. J. Cuccia, S. Saggese, K. M. Kelly, and A. J. Durkin, "Quantitative fluorescence imaging of protoporphyrin IX through determination of tissue optical properties in the spatial frequency domain," J. Biomed. Opt. **16**(12), 126013 (2011).
15. U. Sunar, D. J. Rohrbach, J. Morgan, N. Zeitouni, and B. W. Henderson, "Quantification of PpIX concentration in basal cell carcinoma and squamous cell carcinoma models using spatial frequency domain imaging," Biomed. Opt. Express **4**(4), 531–537 (2013).
16. R. L. Konger, Z. Xu, R. P. Sahu, B. M. Rashid, S. R. Mehta, D. R. Mohamed, S. C. DaSilva-Arnold, J. R. Bradish, S. J. Warren, and Y. L. Kim, "Spatiotemporal assessments of dermal hyperemia enable accurate prediction of experimental cutaneous carcinogenesis as well as chemopreventive activity," Cancer Res. **73**(1), 150–159 (2013).
17. D. J. Rohrbach, D. Muffoletto, J. Huihui, R. Saager, K. Keymel, A. Paquette, J. Morgan, N. Zeitouni, and U. Sunar, "Preoperative mapping of nonmelanoma skin cancer using spatial frequency domain and ultrasound imaging," Acad. Radiol. **21**(2), 263–270 (2014).
18. D. J. Rohrbach, N. C. Zeitouni, D. Muffoletto, R. Saager, B. J. Tromberg, and U. Sunar, "Characterization of nonmelanoma skin cancer for light therapy using spatial frequency domain imaging," Biomed. Opt. Express **6**(5), 1761–1766 (2015).
19. N. E. McKenzie, K. Saboda, L. D. Duckett, R. Goldman, C. Hu, and C. N. Curiel-Lewandrowski, "Development of a photographic scale for consistency and guidance in dermatologic assessment of forearm sun damage," Arch. Dermatol. **147**(1), 31–36 (2011).
20. N. Bodenschatz, A. Brandes, A. Liemert, and A. Kienle, "Sources of errors in spatial frequency domain imaging of scattering media," J. Biomed. Opt. **19**(7), 071405 (2014).
21. J. R. Mourant, T. Fuselier, J. Boyer, T. M. Johnson, and I. J. Bigio, "Predictions and measurements of scattering and absorption over broad wavelength ranges in tissue phantoms," Appl. Opt. **36**(4), 949–957 (1997).
22. R. B. Saager, A. Sharif, K. M. Kelly, and A. J. Durkin, "In vivo isolation of the effects of melanin from underlying hemodynamics across skin types using spatial frequency domain spectroscopy," J. Biomed. Opt. **21**(5), 057001 (2016).
23. M. van de Giessen, J. P. Angelo, and S. Gioux, "Real-time, profile-corrected single snapshot imaging of optical properties," Biomed. Opt. Express **6**(10), 4051–4062 (2015).
24. J. Angelo, C. R. Vargas, B. T. Lee, I. J. Bigio, and S. Gioux, "Ultrafast optical property map generation using lookup tables," J. Biomed. Opt. **21**(11), 110501 (2016).

1. Introduction

With approximately 5.4 million cases diagnosed in the U.S each year, non-melanoma skin cancer (NMSCs), which includes basal cell carcinoma (BCC) and squamous cell carcinoma (SCC), is the most prevalent form of human cancer [1]. At an estimated 5 billion dollars annually, the treatment of NMSC also incurs a significant cost to the healthcare system due to its prevalence. NMSC presents a significant risk of morbidity to the patient especially if it is present in cosmetically sensitive areas such as the face. Moreover, NMSC (especially SCC) can occasionally metastasize, especially in immunosuppressed populations [2]. Typically, clinicians perform a series of examinations during the early stages of the lesion, which includes touching the lesion and visually inspecting it for characteristic symptoms before sending it for biopsy. Once the lesion is determined to be a form of NMSC, the common treatment options are either surgical excision or Mohs micrographic surgery. In contrast, precancerous actinic keratosis (AK) are evaluated clinically (without skin biopsies) and can be treated with destructive modalities (e.g., cryotherapy) or field therapy with topical 5-fluorouracil or topical photodynamic therapy [3]. Evidence suggests that precancerous AK serve as potential precursors for SCC. A study has shown that 97% of SCCs were associated with actinic keratosis, to which the main occurrence of AK is found on elderly individuals with fair skin and a history of excessive sun (UVB) exposure [4]. The key to reducing risk of

Biomedical Optics EXPRESS

morbidity and mortality in NMSC is in the early diagnosis of the pre-cancerous lesion when it progresses from photodamaged skin. Thus, a non-invasive, quick and safe way to qualitatively and quantitatively measure the progress of AKs is desirable among clinicians.

Optical imaging can improve characterization of skin diseases in the early stages so that an appropriate intervention can be applied. Several optical imaging modalities have been applied for imaging skin lesions, including confocal reflectance imaging [5], optical coherence tomography (OCT) [6, 7], spatial frequency domain imaging (SFDI) [8] and laminar optical tomography (LOT) [9–11]. Among mesoscopic diffuse optical imaging techniques, LOT and SFDI are well suited for skin characterization since they provide structural and functional information with relatively high spatial resolution (several hundreds of microns) and depths of a few millimeters.

SFDI is a wide-field, non-contact mesoscopic optical imaging modality that can provide multiple parameters concurrently [12, 13]. In reflectance mode, it can provide maps of optical properties (absorption and scattering) and vascular parameters (hemoglobin concentrations and tissue oxygen saturation) [8]. In fluorescence imaging mode, it can utilize high fluorescence contrast and provide absolute drug fluorescence concentration maps that can allow early detections of premalignant lesions [14, 15]. In this respect, we demonstrated the feasibility of non-invasive quantification of protoporphyrin IX (PpIX) fluorescence concentration distributions in skin tumors [15].

A recent preclinical study has suggested that noninvasive multi-wavelength reflectance-based imaging of skin could detect and monitor precancerous lesions using hemoglobin contrast [16]. One could visualize “hot spots” representing high hemoglobin concentration in areas of skin following a chronic UVB treatment protocol in SKH-1 hairless mice, which progressed to skin cancer. Since SFDI is sensitive to hemoglobin concentration, it can quantify severity of “hot spots”. Previously, we implemented SFDI to quantify optical and vascular parameters in a pilot study of nonmelanoma skin cancers [17] as well as in a larger study [18], which included 17 skin cancer patients. Our data indicated that optical and vascular parameters provided high contrast discriminating tumors from surroundings. These studies also indicated that there exist substantial spatial variations in these parameters.

Here we report results of our pilot study examining SFDI-derived quantitative maps of optical absorption (μ_a) and scattering (μ_s') as well as vascular parameters such as blood oxygen saturation (StO_2) and total hemoglobin concentration (THC) in normal skin vs premalignant lesions from 3 patients with varying degrees of actinic damage.

2. Methods

2.1 Sample selections and clinical assessment

We have initiated a clinical trial under an institutional review board-approved protocol, and informed consent was obtained from all the patients before the measurements. The study is conducted on subjects who are patients in the Wright State University Department of Dermatology clinics in the Wright State Physician’s building. The patients were 35 years old or older with “fair” skin (Fitzpatrick scale I or II), and did not have recent history of use of a tanning bed/significant sun exposure. The three subjects chosen for this pilot study expressed various levels of photodamage, including clinically-apparent AKs for one subject (Fig. 1) characterized by digital photograph [19]. Three wide-field images of both arms were taken from the knuckle (metacarpal-phalangeal) to the elbow to cover the forearm. A 3cm x 4cm area of the subject’s arm was taken and analyzed with SFDI (Fig. 1).

Biomedical Optics EXPRESS

Fig. 1. Clinical pictures of three subjects (P1-3) with increasing levels of photodamage examined by SFDI with the approximate location of the imaged area bounded by the red rectangles.

2.2. SFDI instrumentation and measurements

An SFDI instrument similar to our previous work [17, 18] was implemented (Fig. 2). Three collimated light emitting diodes (LEDs) with center wavelengths of 490nm, 590nm and 660nm (LCS series, Mightex, Toronto, Ontario, Canada) were focused into a liquid light guide and directed onto a digital micromirror device with 1140 x 912 pixel resolution (DLP LightCrafter 4500, Texas Instruments, Dallas, TX). The LEDs were sequentially selected with a four-channel LED controller (SLC-SA04-US, Mightex, Toronto, Ontario, Canada) so that only one wavelength was on at a time. The DMD generated sine wave patterns with 6 different frequencies ranging from 0 to 0.27 mm-1, with three phases (0, $2\pi/3$, $4\pi/3$) for each frequency. The patterns were projected onto the tissue surface and the reflected image was acquired with a sCMOS camera. (Zyla, Andor Technology, Belfast, United Kingdom). Crossed polarizers in front of the camera and DMD rejected any specular reflection. A custom, 3-D printed light shield with an imaging window blocked room light and kept the skin surface at the focal plane of both the DMD and camera. A custom LabView (National Instruments, Austin, TX) program controlled the LED current and camera exposure times.

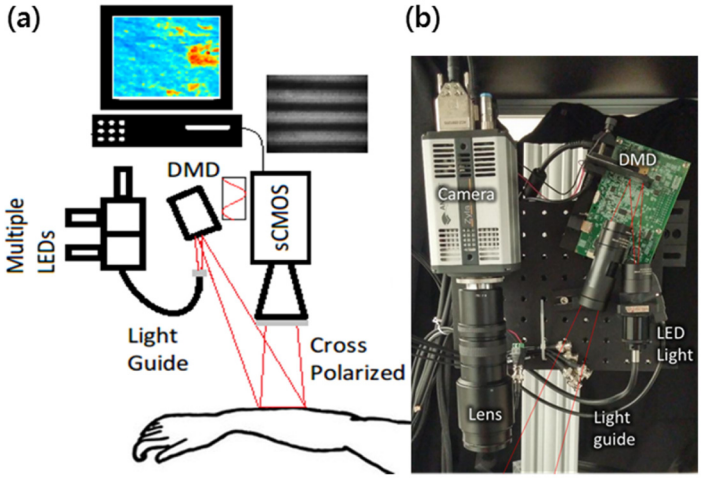

Fig. 2. (a) Schematic diagram and (b) photo of SFDI instrument for imaging lesions on arm.

Biomedical Optics EXPRESS

2.3. SFDI image analysis

For the SFDI analysis, 6 spatial frequencies were used (0 to 0.27 mm^{-1}). For each frequency, the three phases were demodulated to extract the spatially modulated component of the diffuse reflectance [12]. The reflectance data at each pixel were then fit to a Monte Carlo model to quantify absorption (μ_a) and reduced scattering (μ_s') of each lesion. The Monte Carlo model is more appropriate than diffusion approximation in this case since the absorption parameters at 490nm and 590nm were at the same order of magnitude as scattering parameters at these wavelengths [20]. This process was repeated at each wavelength. Tissue scattering was modeled as Mie type behavior, $\mu_s' = A(\lambda/\lambda_0)^{-b}$ where λ0 is the normalization wavelength (700 nm), the parameter A characterizes the magnitude of scattering and b characterizes the wavelength dependence, related to scattering power [21]. Both A and b were determined using a nonlinear algorithm (lsqnonlin, Matlab) to fit the scattering at each pixel to the Mie model.

To obtain the hemoglobin parameters, the absorption parameter was modeled as a linear combination of the primary tissue absorbers, $\mu_a = C_{oxy}\mu^{oxy} + C_{deoxy}\mu^{deoxy} + C_{mel}\mu^{mel} + \mu_a^{back}$. Here μ and C represent the absorption coefficient and concentration of each component (HbO_2, Hb and melanin) respectively, and μaback is assumed to be fixed background absorption coefficient originated from water. The total hemoglobin concentration (THC) and the blood oxygenation saturation (StO_2) maps were calculated from the quantified Coxy (HbO_2) and Cdeoxy (Hb), as THC = Coxy + Cdeoxy, and StO_2 = Coxy/THC.

3. Results and discussion

Figure 3 shows the representative reflectance images at 590nm from 3 patients with visually varying degrees of actinic damage. Patient 1 has much higher reflectance and no visible signs of sun damage. Patient 2 has visible freckles, which might be due to some level of sun damage. Patient 3 has the lowest overall reflectance and also a visible actinic lesion (red arrow).

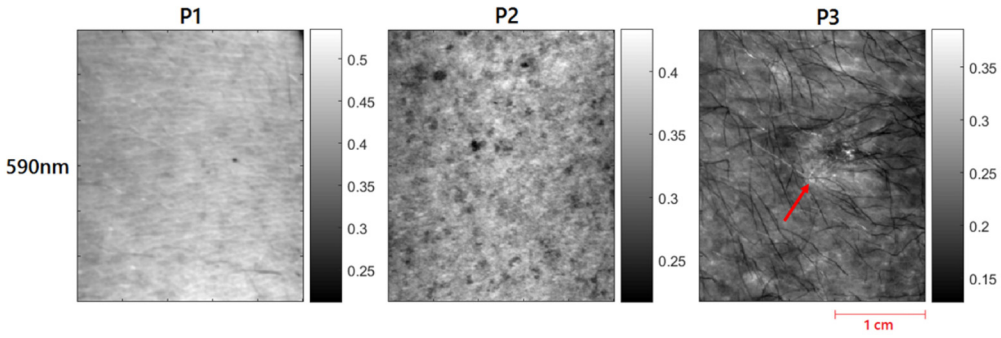

Fig. 3. Reflectance (Rd) images of all three patients at 590nm. Red arrows for patient 3 highlights the visible actinic lesion.

Representative SFDI quantitative images of absorption parameter at 590nm for 3 patients are shown in Figs. 4(a), (b), and (c), respectively. Patient 3 had 152% higher absorption than patient 1 (2.12 ± 0.61cm^{-1} vs. 0.84 ± 0.14 cm^{-1}) In addition, the percent variation for absorption across each image (standard deviation divided by mean, a measure of tissue heterogeneity) was lower for patient 1 and 2 than for patient 3 (16.6%, 14.9% and 28.5%), highlighting the increased heterogeneity for patients 3 due to increasing sun damage score. Figure 4d shows the representative histograms of the optical absorption for each patient, clearly demonstrating the differences in the absorption parameter distributions in these patients.

Biomedical Optics EXPRESS

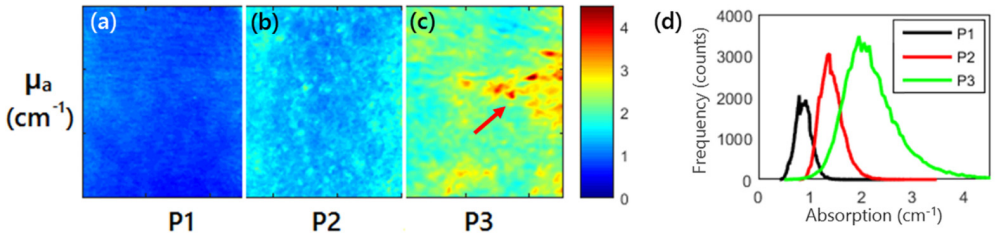

Fig. 4. (a), (b), (c) Absorption imaging maps for all three patients at 590nm. Red arrows highlight the visible lesion for patient 3. (d) Histograms of the absorption parameter for the three patients at 590 nm.

The absorption maps at each wavelength were used to quantify additional physiological parameters including total hemoglobin concentration (THC), blood oxygen saturation (StO_2), concentration on oxy- and deoxy-hemoglobin (Coxy, Cdeoxy) and melanin (Mel). The spatial maps for these parameters are shown in Fig. 5(a) and the histograms are shown in Fig. 5(b). THC increased from patient 1 to patient 3 (1.81 ± 0.22 g/L, 3.6 ± 0.42 g/L and 4.53 ± 1.01 g/L) as did melanin (17.0 ± 4.5 mg/L, 26.6 ± 7.0 mg/L and 42.5 ± 16.6 mg/L). The percent variation in the melanin concentration images were similar for patients 1 and 2 and higher for patient 3 (26%, 26% and 39%), highlighting the increasing sun damage.

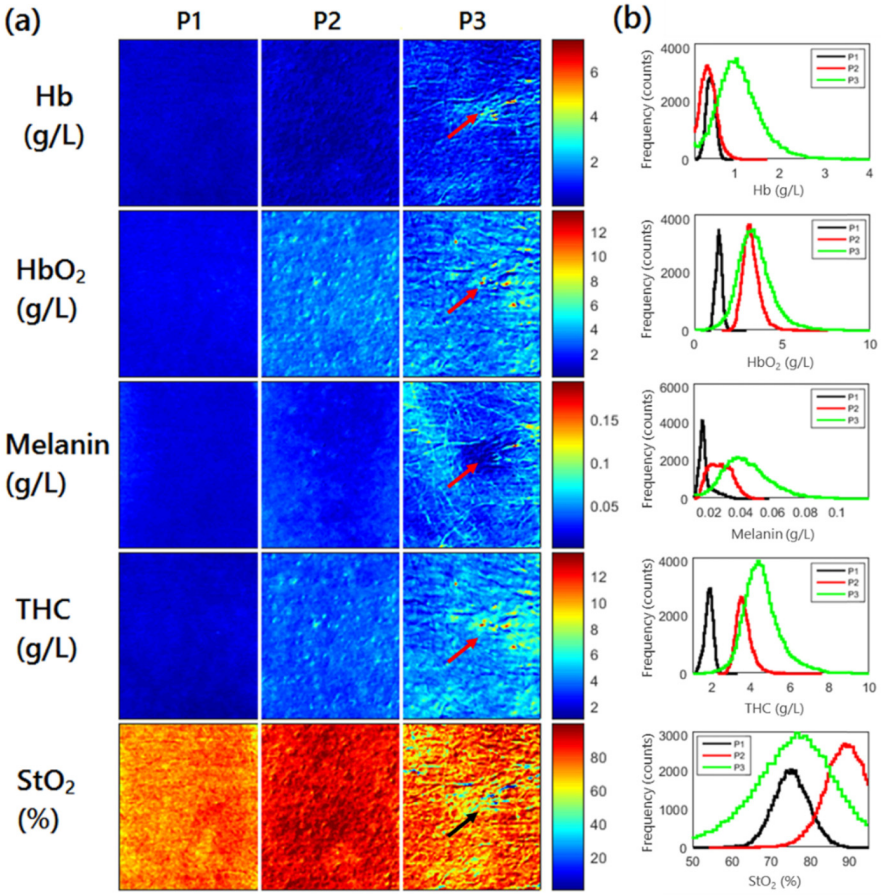

Fig. 5. Physiological parameter quantified from absorption maps. (a) shows the spatial maps for each parameter for each patient. Arrows highlight the visible lesion for patient 3. (b) shows the summary histogram of each parameter.

Biomedical Optics EXPRESS

Representative SFDI quantitative images of the scattering parameter at 590nm for 3 patients are shown in Figs. 6(a), (b), and (c), respectively. Compared to patient 1, patient 3 had 42% lower reduced scattering (14.4 ± 3.4 cm^{-1} vs. 24.7 ± 2.4 cm^{-1}) with patient 2 falling in between (20.9 ± 2.2 cm^{-1}). In addition, the percent variation across each image (standard deviation divided by mean, a measure of tissue heterogeneity) increased from patient 1 to patient 3 for reduced scattering (9.7%, 10.5% and 23.6%), highlighting the increased heterogeneity for patients 2 and 3 due to increasing sun damage score.

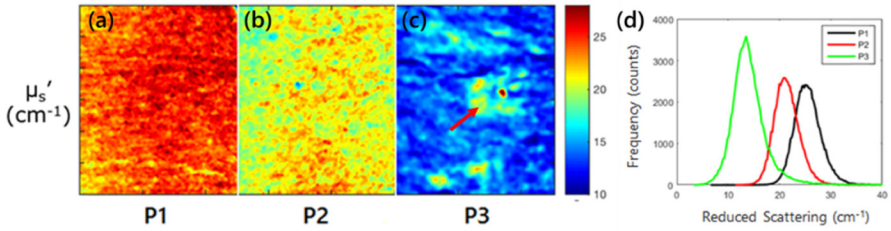

Fig. 6. (a), (b), (c) Scattering imaging maps for all three patients at 590nm. Red arrows highlight the visible lesion for patient 3. (d) Histograms of the scattering parameter for the three patients at 590 nm.

The reduced scattering maps at each wavelength were used to quantify parameters relating to tissue structure including the scattering magnitude (A) and scattering power (b). The spatial maps for these parameters are shown in Fig. 7(a) for each patient and the combined histograms are shown in Fig. 7(b). While the average value for the scattering parameter b did not show a trend between patients (0.58 ± 0.19, 0.22 ± 0.21 and 0.27 ± 0.42), the percent variation for the images did (33%, 95% and 156%), illustrating that the image heterogeneity may be another key parameter to characterize lesion severity.

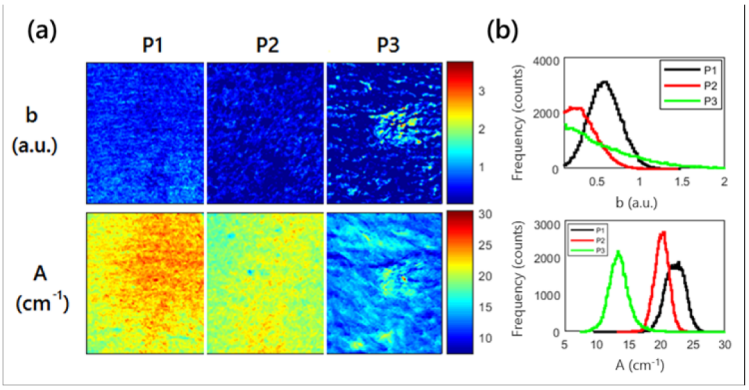

Fig. 7. Scattering amplitude, A, and power, b, maps. (a) shows the spatial maps for each parameter for each patient. Red arrows highlight the visible lesion for patient 3. (b) shows the summary histogram of each parameter.

In this study, only three wavelengths were used for multiwavelength fitting due to availability of the light sources in our instrument. We acknowledge that the use of fewer wavelengths may result is less stable fitting and therefore the quantification of physiological parameters such as oxy-, deoxy-hemoglobin and melanin may suffer. Melanin in particular can be a difficult absorber to quantify due to its featureless absorption spectrum and uneven distribution in the skin [18, 22]. Although hemodynamic parameters may not show as much difference as the optical properties for these patients, these are useful physiological parameters related to disease progression and may show differences for other patients, each

Biomedical Optics EXPRESS

parameter and the combination thereof can show different sensitivity and specificity for individual patient. We may be more prone to errors in quantification of physiological parameters due to few number of LED sources available in our current instrument, thus adding more wavelengths may allow more accurate quantification and thereby better contrasts. We plan to add more LEDs at different wavelengths such as 630nm and 740nm, which would increase the number of wavelength to 5 for improved quantification of concentrations.

It should be also noted that all the reported values were obtained via post-processing with custom MATLAB software that fit the data to the model at each pixel. This process took between 5 and 10 minutes depending on the pixel binning and was performed outside the clinic. In total, the data acquisition time in the clinic was around 1 minute, and pixel by pixel fitting for optical properties took 1-2 minute per wavelength and the multi-wavelength fitting took 2-3 minutes. These times could be reduced by binning to fit fewer pixels. Utilizing a faster acquisition technique such as single snapshot [23] or a faster processing technique such as the look up table (LUT) model recently proposed by Angelo *et. al* [24] could reduce the overall quantification time and provide results in the clinic. This near real-time feedback would be particularly useful for monitoring light-based therapies such as laser or photodynamic therapy.

4. Conclusion

This pilot study indicates that SFDI can provide quantitative maps of optical and vascular parameters of precancerous lesions such as actinic keratosis in humans, with increased scattering and total hemoglobin concentration with respect to lesion stage. By frequent monitoring of these patients, we will be able to provide additional feedback on the progress of the pre-cancerous lesions turning malignant.

Funding

Ohio Third Frontier to the Ohio Imaging Research and Innovation Network (OIRAIN) (667750); National Institutes of Health (NIH) (HL062996, ES020866, AG048946, AR070010); and Veteran's Administration Merit Award (1101CX000809).